Two New Sum-of-Sinusoids-Based Methods for the Efficient Generation of Multiple Uncorrelated Rayleigh Fading Waveforms

Matthias Pätzold, *Senior Member, IEEE,* Cheng-Xiang Wang, *Senior Member, IEEE,* and Bjørn Olav Hogstad

Abstract—This paper deals with the design of a set of multiple uncorrelated Rayleigh fading waveforms. The Rayleigh fading waveforms are mutually uncorrelated, but each waveform is correlated in time. The waveforms are generated by using the deterministic sum-of-sinusoids (SOS) channel modeling principle. Two new closed-form solutions are presented for the computation of the model parameters. Analytical and numerical results show that the resulting deterministic SOS-based channel simulator fulfills all main requirements imposed by the reference model with given correlation properties derived under two-dimensional isotropic scattering conditions. The proposed methods are useful for the design of simulation models for diversity-combined Rayleigh fading channels, relay fading channels, frequency-selective channels, and multiple-input multiple-output (MIMO) channels.

Index Terms—Uncorrelated Rayleigh fading waveforms, deterministic sum-of-sinusoids channel simulator, parameter computation method, statistics.

I. INTRODUCTION

THE generation of a set of multiple uncorrelated Rayleigh fading waveforms is important for the development and analysis of diversity schemes, wideband wireless communication systems, and multiple-input multiple-output (MIMO) techniques. The design of channel simulators enabling the accurate and efficient generation of multiple uncorrelated Rayleigh fading processes has therefore been the subject of research for many years. The sum-of-sinusoids (SOS) principle, originally introduced in [1], [2], has widely been applied to the development of simulation models for Rayleigh fading channels [3]–[24]. To generate multiple uncorrelated Rayleigh fading waveforms by using SOS channel simulators, many different parameter computation methods [3]–[16] have

been investigated. In general, the SOS channel simulators can be classified as deterministic [3]–[12], ergodic stochastic, or non-ergodic stochastic [12]–[16] depending on the underlying parameter computation methods. A deterministic SOS channel simulator has constant model parameters (gains, frequencies, and phases) for all simulation trials. An ergodic stochastic SOS channel simulator has constant gains and frequencies but random phases [17]. Due to the ergodic property, it needs only one simulation trial to represent its complete statistical properties. A sample function, i.e., a single simulation trial of a stochastic SOS channel simulator actually results in a deterministic process (waveform). Thus, we can also say that a deterministic channel simulator can be used to generate sample functions of a stochastic process. A non-ergodic stochastic SOS channel simulator assumes that the frequencies and/or gains are random variables. The statistical properties of a non-ergodic stochastic SOS channel simulator vary for each simulation trial and have to be calculated by averaging over a large number of simulation trials. Both ergodic stochastic (deterministic) and non-ergodic stochastic SOS channel simulators have pros and cons, which have been discussed, e.g., in [11], [12]. Deterministic SOS channel simulators generally have a higher efficiency compared to non-ergodic stochastic SOS channel simulators [18].

Although Jakes' deterministic SOS channel simulator [3] is widely in use, it has some undesirable properties. One of them comes from the non-zero cross-correlation function (CCF) of the inphase and quadrature components of the generated complex waveforms. In [3], Jakes proposed also an extension of his approach aiming to generate K multiple uncorrelated waveforms, but it was shown in [4] that the CCF between any pair of generated complex waveforms can be quite large. Dent *et al.* [5] suggested a modification to Jakes' method by using orthogonal Walsh-Hadamard matrices to decorrelate the generated waveforms. This reduces the CCFs but they are still not exactly zero. The same problem of non-zero CCFs between different waveforms is retained for the deterministic method proposed in [6]. Another deterministic method that enables the generation of a set of K mutually uncorrelated Rayleigh fading waveforms was introduced in [7]. Using this method, the temporal autocorrelation function (ACF) of each of the K underlying complex waveforms is very close to the specified one. Unfortunately, this is not the case for the ACFs of the inphase and quadrature parts of the designed complex waveforms. In [12], both a deterministic and a stochastic

method were suggested aiming to tackle the problem of designing multiple uncorrelated Rayleigh fading waveforms. However, when applying the deterministic method, the ACFs of the inphase and quadrature parts of the generated complex waveforms are quite different from the corresponding ACFs of the reference model—even if the number of sinusoidal terms tends to infinity—and the proposed stochastic method results in a non-ergodic channel simulator. The L_p-norm method [8]–[10] is very powerful and not limited to isotropic channels, but it lacks a simple closed-form solution and requires professional experience in numerical optimization techniques to achieve the expected results. The usefulness of the method of exact Doppler spread (MEDS) [19] concerning the generation of multiple uncorrelated Rayleigh fading processes with a deterministic SOS channel simulator was revisited in [9], [10]. There it was shown that all the main requirements can be fulfilled, but unfortunately the complexity of the resulting channel simulator increases almost exponentially with the increase of the number of uncorrelated waveforms. This makes the original MEDS less efficient if the number of uncorrelated waveforms is large.

Non-ergodic stochastic methods, such as those proposed in [12]–[16], can be used to guarantee that the CCFs of different waveforms are zero, but the temporal ACF of the waveform obtained from a single simulation trial is generally not sufficiently close to the desired ACF of the reference model. This problem can only be solved by averaging over many simulation trials, which reduces the efficiency of the approach. Considering all the pros and cons of the existing methods in [3]–[10], [12]–[16] that have been proposed by many researchers over several decades, one must come to the conclusion that a better solution to the problem of designing multiple uncorrelated Rayleigh fading waveforms with a better tradeoff between the model accuracy and simulation efficiency is still desirable.

In this paper, we present two deterministic solutions of the problem. For the first time, we introduce a generalized version of the MEDS. This generalized version can be interpreted as a class of parameter computation methods, which includes many other well-known approaches as special cases. Two new special cases are introduced here, each of which enables the efficient and accurate design of multiple uncorrelated Rayleigh fading waveforms using deterministic concepts. Our proposed methods can fulfill all main requirements imposed on the correlation properties of the resulting channel simulator. Also, they keep the model complexity low and provide simple closed-form solutions for the computation of the model parameters.

The rest of this paper is organized as follows. Section II describes the problem and the conditions that must be fulfilled to obtain K mutually uncorrelated Rayleigh fading waveforms using an SOS channel simulator. In Section III, a new class of parameter computation methods is introduced, which then provides two closed-form solutions of the problem under the conditions of isotropic scattering. In Section IV, it is shown that the new class of parameter computation methods includes several other well-known methods as special cases. Section V provides a comparison and discussion of the proposed new methods. Finally, the conclusions are drawn in Section VI.

II. PROBLEM DESCRIPTION

We want to simulate K mutually uncorrelated Rayleigh fading waveforms

$$\tilde{\zeta}^{(k)}(t)=|\tilde{\mu}^{(k)}(t)|=|\tilde{\mu}_1^{(k)}(t)+j\tilde{\mu}_2^{(k)}(t)|, \; k=1,2,\ldots,K \quad (1)$$

by using an SOS channel simulator, which generates the waveforms

$$\tilde{\mu}_i^{(k)}(t)=\sqrt{\frac{2}{N_i}}\sum_{n=1}^{N_i}\cos(2\pi f_{i,n}^{(k)}t+\theta_{i,n}^{(k)}), \quad i=1,2 \quad (2)$$

where $j=\sqrt{-1}$, N_i denotes the number of sinusoids, $f_{i,n}^{(k)}$ is called the discrete Doppler frequency, and $\theta_{i,n}^{(k)}$ is the phase of the nth sinusoid of the inphase component $\tilde{\mu}_1^{(k)}(t)$ or quadrature component $\tilde{\mu}_2^{(k)}(t)$ of the kth complex waveform $\tilde{\mu}^{(k)}(t)$. The phases $\theta_{i,n}^{(k)}$ are considered as outcomes of independent and identically distributed (i.i.d.) random variables $\boldsymbol{\theta}_{i,n}^{(k)}$, each having a uniform distribution over the interval $(0, 2\pi]$. For increased clarity, the structure of the SOS channel simulator is shown in Fig. 1.

For given sets of constant model parameters $\{f_{i,n}^{(k)}\}$ and $\{\theta_{i,n}^{(k)}\}$, the time-averaged ACF $\tilde{r}_{\mu_i\mu_i}^{(k)}(\tau)$ of the kth waveform $\tilde{\mu}_i^{(k)}(t)$ can be expressed as [8]

$$
\begin{aligned}
\tilde{r}_{\mu_i\mu_i}^{(k)}(\tau) &= <\tilde{\mu}_i^{(k)}(t)\tilde{\mu}_i^{(k)}(t+\tau)> \\
&= \lim_{T\to\infty}\frac{1}{2T}\int_{-T}^{T}\tilde{\mu}_i^{(k)}(t)\tilde{\mu}_i^{(k)}(t+\tau)\,dt \\
&= \frac{1}{N_i}\sum_{n=1}^{N_i}\cos(2\pi f_{i,n}^{(k)}\tau) \quad (3)
\end{aligned}
$$

for $i=1,2$ and $k=1,2,\ldots,K$. Analogously, the time-averaged CCF $\tilde{r}_{\mu_i\mu_\lambda}^{(k,l)}(\tau)$ of $\tilde{\mu}_i^{(k)}(t)$ and $\tilde{\mu}_\lambda^{(l)}(t)$ can be obtained as in (4) [8], [9] for $i,\lambda=1,2$ and $k,l=1,2,\ldots,K$. The

$$
\begin{aligned}
\tilde{r}_{\mu_i\mu_\lambda}^{(k,l)}(\tau) &= <\tilde{\mu}_i^{(k)}(t)\,\tilde{\mu}_\lambda^{(l)}(t+\tau)> = \lim_{T\to\infty}\frac{1}{2T}\int_{-T}^{T}\tilde{\mu}_i^{(k)}(t)\,\tilde{\mu}_\lambda^{(l)}(t+\tau)\,dt \\[2mm]
&= \begin{cases} \dfrac{1}{\sqrt{N_iN_\lambda}}\displaystyle\sum_{n=1}^{N_i}\sum_{m=1}^{N_\lambda}\cos(2\pi f_{i,n}^{(k)}\tau-\theta_{i,n}^{(k)}\pm\theta_{\lambda,m}^{(\ell)}), & \text{if } f_{i,n}^{(k)}=\pm f_{\lambda,m}^{(\ell)} \\[4mm] 0, & \text{if } f_{i,n}^{(k)}\neq\pm f_{\lambda,m}^{(\ell)} \end{cases}
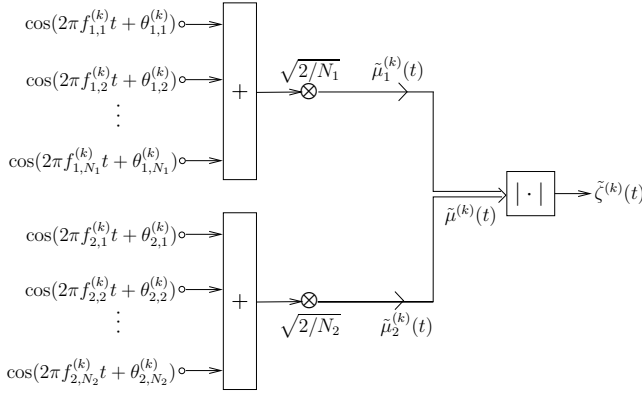\end{aligned} \quad (4)
$$

Fig. 1.   Structure of the SOS channel simulator for Rayleigh fading waveforms.

problem is to find proper values for the discrete Doppler frequencies $f_{i,n}^{(k)}$ in such a way that the following two conditions are fulfilled:

(i) The ACF $\tilde{r}_{\mu_i\mu_i}^{(k)}(\tau)$ of the simulation model must be as close as possible to the ACF $r_{\mu_i\mu_i}(\tau)$ of a given reference model over a certain domain, i.e.,

$$\tilde{r}_{\mu_i\mu_i}^{(k)}(\tau) \approx r_{\mu_i\mu_i}(\tau), \quad \forall\, \tau \in [0,\,\tau_{\max}] \tag{5}$$

where $\tau_{\max}$ denotes the maximum time lag that determines the domain over which the quality of the approximation is of interest. To measure the quality of the approximation $\tilde{r}_{\mu_i\mu_i}^{(k)}(\tau) \approx r_{\mu_i\mu_i}(\tau)$ over the interval $[0,\,\tau_{\max}]$, we use the following L_2-norm

$$E_2 = \left[\frac{1}{\tau_{\max}} \int_0^{\tau_{\max}} |\tilde{r}_{\mu_i\mu_i}^{(k)}(\tau) - r_{\mu_i\mu_i}(\tau)|^2 d\tau \right]^{1/2}. \tag{6}$$

(ii) The CCFs $\tilde{r}_{\mu_i\mu_\lambda}^{(k,l)}(\tau)$ of $\tilde{\mu}_i^{(k)}(t)$ and $\tilde{\mu}_\lambda^{(l)}(t)$ must be equal to zero, i.e.,

$$\tilde{r}_{\mu_i\mu_\lambda}^{(k,l)}(\tau) = 0, \quad \forall \tau, \quad i \neq \lambda \tag{7a}$$

$$\tilde{r}_{\mu_i\mu_i}^{(k,l)}(\tau) = 0, \quad \forall \tau, \quad k \neq l \tag{7b}$$

where $i, \lambda = 1, 2$ and $k, l = 1, 2, \ldots, K$.

It is worth noting that the above conditions should be fulfilled by keeping the complexity of the simulation model to a minimum, which means that N_i must be as small as possible.

By considering the CCF $\tilde{r}_{\mu_i\mu_\lambda}^{(k,l)}(\tau)$ in (4), we may conclude that (7a) and (7b) can be guaranteed if and only if

$$f_{i,n}^{(k)} \neq \pm f_{\lambda,m}^{(l)}, \quad i \neq \lambda \tag{8a}$$

$$f_{i,n}^{(k)} \neq \pm f_{i,n}^{(l)}, \quad k \neq l \tag{8b}$$

hold, respectively, for all $n = 1, 2, \ldots, N_i$ and $m = 1, 2, \ldots, N_\lambda$. The above two equations state that the sets of discrete Doppler frequencies of different waveforms $\tilde{\mu}_i^{(k)}(t)$ and $\tilde{\mu}_j^{(l)}(t)$ must be disjoint, i.e., $\{f_{i,n}^{(k)}\}_{n=1}^{N_i} \cap \{f_{\lambda,m}^{(l)}\}_{m=1}^{N_\lambda} = \{\emptyset\}$ if $i \neq \lambda$ $(i, \lambda = 1, 2)$ and $k \neq l$ $(k, l = 1, 2, \ldots, K)$, where $\{\emptyset\}$ denotes the empty set.

Since it follows from (7a) that the CCFs $\tilde{r}_{\mu_1\mu_2}^{(k,k)}(\tau)$ and $\tilde{r}_{\mu_2\mu_1}^{(k,k)}(\tau)$ are zero, we can express the ACF $\tilde{r}_{\mu\mu}^{(k)}(\tau)$ of the

kth complex waveform $\tilde{\mu}^{(k)}(t) = \tilde{\mu}_1^{(k)}(t) + j\tilde{\mu}_2^{(k)}(t)$ as

$$\tilde{r}_{\mu\mu}^{(k)}(\tau) = \tilde{r}_{\mu_1\mu_1}^{(k)}(\tau) + \tilde{r}_{\mu_2\mu_2}^{(k)}(\tau). \tag{9}$$

In this paper, we will restrict our reference model to the Rayleigh model under two-dimensional isotropic scattering conditions [3], [20]. Recall that the ACF $r_{\mu_i\mu_i}(\tau)$ of the reference model is given by

$$r_{\mu_i\mu_i}(\tau) = J_0(2\pi f_{\max}\tau), \quad i = 1, 2 \tag{10}$$

where $J_0(\cdot)$ denotes the zeroth-order Bessel function of the first kind and $f_{\max}$ is the maximum Doppler frequency. In this case, the ACF of the complex process $\mu(t) = \mu_1(t) + j\mu_2(t)$ equals $r_{\mu\mu}(\tau) = 2r_{\mu_i\mu_i}(\tau) = 2J_0(2\pi f_{\max}\tau)$, since the CCFs $r_{\mu_1\mu_2}(\tau)$ and $r_{\mu_2\mu_1}(\tau)$ are zero.

III. PROBLEM SOLUTIONS

To solve the problem described in Section II, we propose the generalized MEDS (GMEDS$_q$). According to this method, the discrete Doppler frequencies $f_{i,n}^{(k)}$ are given by

$$\begin{aligned} f_{i,n}^{(k)} &= f_{\max}\cos(\alpha_{i,n}^{(k)}) \\ &= f_{\max}\cos\left[\frac{q\pi}{2N_i}\left(n - \frac{1}{2} \right) + \alpha_{i,0}^{(k)} \right] \end{aligned} \tag{11}$$

where $\alpha_{i,0}^{(k)}$ is called the angle of rotation that will be defined subsequently and $q \in \{0, 1, 2\}$. Note that the quantity q mainly determines the range of values for the angles of arrival $\alpha_{i,n}^{(k)}$. Empirical studies have shown that for the GMEDS$_q$, the quantity $\tau_{\max}$ in (6) is given by $\tau_{\max} = N_i/(2qf_{\max})$ when $q = 1, 2$. From (11), it is clear that the GMEDS$_q$ reduces to the original MEDS if $q = 1$ and $\alpha_{i,0}^{(k)} = 0$.

A. The GMEDS$_1$

In the following, we show how the GMEDS$_1$ can be used to generate any number K of multiple uncorrelated Rayleigh fading waveforms. According to the GMEDS$_1$, the discrete Doppler frequencies $f_{i,n}^{(k)}$ are obtained from (11) by setting q to 1 and defining the angle of rotation $\alpha_{i,0}^{(k)}$ as

$$\alpha_{i,0}^{(k)} := (-1)^{i-1}\frac{\pi}{4N_i} \cdot \frac{k}{K+2} \tag{12}$$

where $i = 1, 2$ and $k = 1, 2, \ldots, K$. It follows an analysis of the GMEDS$_1$ with some background information that clarifies the motivation for introducing (12).

For this purpose, we start from (11) with $q = 1$ and substitute (3) and (10) in (6), which allows us to study the influence of the angle of rotation $\alpha_{i,0}^{(k)}$ on the quality of the approximation in (5). The behavior of the error function $E_2 = E_2(\alpha_{i,0}^{(k)})$ as a function of $\alpha_{i,0}^{(k)}$ is illustrated in Fig. 2 for various values of N_i. Clearly, with an increase of N_i, $E_2(\alpha_{i,0}^{(k)})$ can be reduced. It can also be observed that the error function $E_2(\alpha_{i,0}^{(k)})$ is periodic with period $\alpha_{\mathrm{per}} = \pi/2$, i.e., $E_2(\alpha_{i,0}^{(k)}) = E_2(\alpha_{i,0}^{(k)} + p\pi/2)$, where p stands for an integer. Moreover, $E_2(\alpha_{i,0}^{(k)})$ is almost even symmetrical, i.e., $E_2(\alpha_{i,0}^{(k)}) \approx E_2(-\alpha_{i,0}^{(k)})$. The minimum and maximum values of $E_2(\alpha_{i,0}^{(k)})$ are obtained when $\alpha_{i,0}^{(k)}$ equals $p\alpha_{\mathrm{per}}$ and $(2p+1)\alpha_{\mathrm{per}}/2$, respectively.
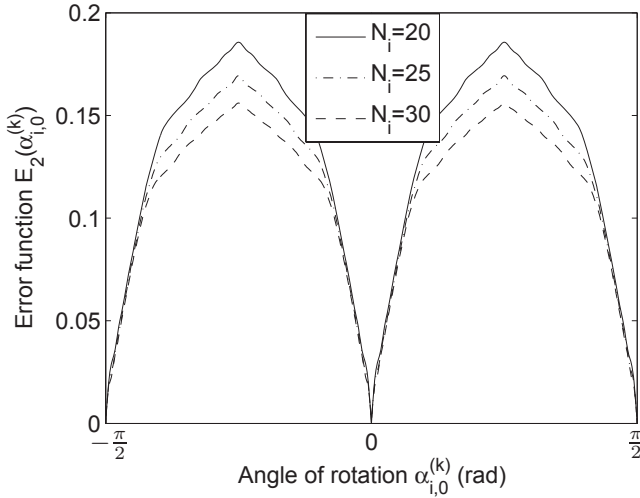
Fig. 2. The error function $E_2 = E_2(\alpha_{i,0}^{(k)})$ as a function of $\alpha_{i,0}^{(k)}$ by using the GMEDS$_1$ for various values of N_i.

Hence, the original MEDS ($q = 1$, $\alpha_{i,0}^{(k)} = 0$) results in the best fitting to the quadrature ACF $r_{\mu_i\mu_i}(\tau)$. A nice property of the original MEDS is that $E_2(0) \to 0$ as $N_i \to \infty$ [19]. For a limited number of N_i, the value of $E_2(0)$ is different from zero. An idea of how fast $E_2(0)$ approaches zero can be gathered from the plot in [8, Fig. 5.45], where the mean-square error of $\tilde{r}_{\mu_i\mu_i}(\tau)$ is shown as a function of N_i. From the inspection of Fig. 2, we also note that large approximation errors may occur if $\alpha_{i,0}^{(k)} \neq p\pi/2$. This fact holds even for large values of N_i. In what follows, we will investigate the conditions we have to impose on $\alpha_{i,0}^{(k)}$, so that (8a) and (8b) can be satisfied.

Since $1 \leq n \leq N_i$, we may conclude that $\frac{\pi}{4N_i} \leq \frac{\pi}{2N_i}(n - \frac{1}{2}) \leq \frac{\pi}{2} - \frac{\pi}{4N_i}$ holds. If we limit the values of $\alpha_{i,0}^{(k)}$ in (11) to the interval $[-\frac{\pi}{4N_i}, \frac{\pi}{4N_i}]$ with $N_i < \infty$, we may further write $\alpha_{i,n}^{(k)} \in [0, \pi/2]$. Within this range, it follows from (11) that the discrete Doppler frequencies $f_{i,n}^{(k)}$ are monotonically decreasing quantities over the interval $[0, f_{max}]$ with increasing values of n, i.e., $0 \leq f_{i,n+1}^{(k)} < f_{i,n}^{(k)} \leq f_{max}$. For simplicity, let $N_1 = N_2$. Then, (8a) and (8b) can always be fulfilled if and only if

$$\alpha_{i,0}^{(k)} \neq \alpha_{\lambda,0}^{(l)} - \frac{\pi(n-m)}{2N_i}, \quad i \neq \lambda \quad (13a)$$

$$\alpha_{i,0}^{(k)} \neq \alpha_{i,0}^{(l)}, \quad\quad\quad k \neq l \quad (13b)$$

hold, respectively, for all $n, m = 1, 2, \ldots, N_i$, where $k, l = 1, 2, \ldots, K$ and $i, \lambda = 1, 2$. The above conditions are sufficient to guarantee that the CCFs $\tilde{r}_{\mu_i\mu_\lambda}^{(k,l)}(\tau)$ of $\tilde{\mu}_i^{(k)}(t)$ and $\tilde{\mu}_\lambda^{(l)}(t)$ are equal to 0, i.e., (7a) and (7b) will follow.

There are a number of ways to satisfy the conditions (13a) and (13b) and to design a set of K mutually uncorrelated Rayleigh fading waveforms. In this paper, we define the angle of rotation $\alpha_{i,0}^{(k)}$ as in (12). Note that $\alpha_{i,0}^{(k)} \in (0, \pi/(4N_i))$ for $i = 1$ while $\alpha_{i,0}^{(k)} \in (-\pi/(4N_i), 0)$ for $i = 2$. For the GMEDS$_1$, the worst approximation result of the ACF $\tilde{r}_{\mu_i\mu_i}^{(k)}(\tau)$ is obtained if $k = K$, i.e., $\alpha_{i,0}^{(k)} = \alpha_{i,0}^{(K)} = \pm\frac{\pi}{4N_i}\frac{K}{K+2}$, no matter of the value chosen for K. In contrast to the MEDS,

the introduction of the angle of rotation $\alpha_{i,0}^{(k)}$ in (11) guarantees that the conditions in (8a) and (8b) can be satisfied without choosing different values for N_i. In this sense, the GMEDS$_1$ removes the constraint on N_i. Consequently, a very large number (theoretically infinite) K of mutually uncorrelated Rayleigh fading waveforms $\tilde{\zeta}^{(k)}(t)$ ($k = 1, 2, \ldots, K$) can be designed by using (12) without increasing the model complexity determined by N_i.

Following the above discussion, the inequality $\frac{\pi}{2N_i}(n - \frac{1}{2}) + \alpha_{i,0}^{(k)} > \frac{\pi}{2N_i}(n - \frac{1}{2})$ holds if $0 < \alpha_{i,0}^{(k)} < \pi/(4N_i)$. In this case, $f_{i,n}^{(k)}$ in (11) is always smaller for the GMEDS$_1$ than the corresponding $f_{i,n}^{(k)}$ for the MEDS with $\alpha_{i,0}^{(k)} = 0$. From (3), it now becomes clear that when using the GMEDS$_1$ then the ACF $\tilde{r}_{\mu_i\mu_i}^{(k)}(\tau)$ is always larger than or equal to $\tilde{r}_{\mu_i\mu_i}(\tau)$ obtained by applying the MEDS over a certain interval $\tau \in [0, \tau_{max}]$. The opposite statement holds if $-\pi/(4N_i) < \alpha_{i,0}^{(k)} < 0$. For the MEDS, it is important to mention that $\tilde{r}_{\mu_i\mu_i}(\tau)$ is very close to $r_{\mu_i\mu_i}(\tau) = J_0(2\pi f_{max}\tau)$ over the interval $\tau \in [0, \tau_{max}]$ with $\tau_{max} = N_i/(2f_{max})$, as demonstrated in Fig. 2. Consequently, we obtain the following important properties for the ACF $\tilde{r}_{\mu_i\mu_i}^{(k)}(\tau)$ of the GMEDS$_1$:

$$\tilde{r}_{\mu_i\mu_i}^{(k)}(\tau) \geq r_{\mu_i\mu_i}(\tau), \quad \text{if} \quad 0 < \alpha_{i,0}^{(k)} < \pi/(4N_i) \quad (14a)$$

$$\tilde{r}_{\mu_i\mu_i}^{(k)}(\tau) \leq r_{\mu_i\mu_i}(\tau), \quad \text{if} \quad -\pi/(4N_i) < \alpha_{i,0}^{(k)} < 0 \quad (14b)$$

where $\tau \in [0, \tau_{max}]$ and $\tau_{max} = N_i/(2f_{max})$. These results can be phrased as follows. A positive (or negative) angle of rotation $\alpha_{i,0}^{(k)} \in (0, \pi/(4N_i))$ (or $\alpha_{i,0}^{(k)} \in (-\pi/(4N_i), 0)$) always results in non-negative (or non-positive) errors of the ACF $\tilde{r}_{\mu_i\mu_i}^{(k)}(\tau)$ of the simulation model with respect to the ACF $r_{\mu_i\mu_i}(\tau)$ of the reference model within the interval $\tau \in [0, \tau_{max}]$.

The above property is confirmed by the results shown in Fig. 3, where plots of the ACFs $\tilde{r}_{\mu_i\mu_i}^{(k)}(\tau)$ obtained by applying the MEDS ($\alpha_{i,0}^{(k)} = 0$) and the GMEDS$_1$ for two selected values of $\alpha_{i,0}^{(k)}$ according to (12) with $N_i = 20$, and $k = K = 4$ are presented. For comparison, this figure also illustrates the behavior of the ACF $r_{\mu_i\mu_i}(\tau)$ of the reference model. Obviously, the best fitting is obtained when the original MEDS is used. In this case, the approximation $\tilde{r}_{\mu_i\mu_i}^{(k)}(\tau) \approx r_{\mu_i\mu_i}(\tau)$ is excellent if $\tau \in [0, N_i/(2f_{max})]$, i.e., $\tau f_{max} \in [0, 10]$. It can also be observed that if $\alpha_{i,0}^{(k)} = \pi/120$, then $\tilde{r}_{\mu_i\mu_i}^{(k)}(\tau) \geq r_{\mu_i\mu_i}(\tau)$ holds for $\tau f_{max} \in [0, 10]$. The opposite conclusion is obtained if $\alpha_{i,0}^{(k)} = -\pi/120$. Note that Fig. 3 shows the worst approximation result of the ACF $\tilde{r}_{\mu_i\mu_i}^{(k)}(\tau)$ for the GMEDS$_1$ when $\alpha_{i,0}^{(k)} = \pm\pi/120$, which follows from (12) if $k = K$. For $k < K$, the approximation results are much better, which is also clear from Fig. 2. A comparative study has revealed that even the worst case of the GMEDS$_1$ provides better approximation results regarding the ACF $r_{\mu_i\mu_i}(\tau)$ than many other methods, including Jakes' method in [3], the deterministic methods in [5]–[7], and the random methods in [12]–[15] with respect to single trials. From (12) and (14), we can further conclude that the inphase ACF $\tilde{r}_{\mu_1\mu_1}^{(k)}(\tau)$ with $\alpha_{1,0}^{(k)}$ always has non-negative errors, while the quadrature ACF $\tilde{r}_{\mu_2\mu_2}^{(k)}(\tau)$ with $\alpha_{2,0}^{(k)} = -\alpha_{1,0}^{(k)}$ always has non-positive errors over the interval $\tau \in [0, \tau_{max}]$. Recall from Fig. 2 that the error
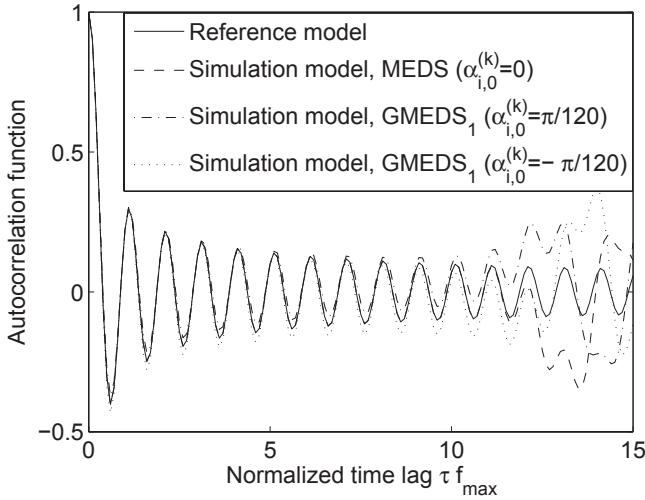
Fig. 3. The ACFs of the quadrature components of the reference model $r_{\mu_i \mu_i}(\tau)$ and the simulation model $\tilde{r}_{\mu_i \mu_i}^{(k)}(\tau)$ by using the MEDS with $\alpha_{i,0}^{(k)} = 0$ and GMEDS$_1$ with $\alpha_{i,0}^{(k)} = \pm \pi/120$ ($N_i = 20$, $K = 4$).

Fig. 4. The error function $E_2'(\alpha_{i,0}^{(k)})$ as a function of $\alpha_{i,0}^{(k)}$ by using the GMEDS$_1$ for various values of N_i.

function $E_2(\alpha_{i,0}^{(k)})$ is almost even symmetrical. This means that the non-negative and non-positive errors of $\tilde{r}_{\mu_1 \mu_1}^{(k)}(\tau)$ and $\tilde{r}_{\mu_2 \mu_2}^{(k)}(\tau)$, respectively, compensate each other in such a way that the approximation of $\tilde{r}_{\mu \mu}^{(k)}(\tau) = \tilde{r}_{\mu_1 \mu_1}^{(k)}(\tau) + \tilde{r}_{\mu_2 \mu_2}^{(k)}(\tau)$ to $r_{\mu \mu}(\tau) = 2J_0(2\pi f_{\max}\tau)$ is excellent at least over the domain $[0, \tau_{\max}]$, where $\tau_{\max} = N_i/(2f_{\max})$. Similar to (6), the quality of the approximation $\tilde{r}_{\mu \mu}^{(k)}(\tau) \approx r_{\mu \mu}(\tau)$ over the interval $[0, \tau_{\max}]$ can be measured by using the following L_2-norm

$$E_2'(\alpha_{i,0}^{(k)}) = \left[\frac{1}{\tau_{\max}} \int_0^{\tau_{\max}} |\tilde{r}_{\mu \mu}^{(k)}(\tau) - r_{\mu \mu}(\tau)|^2 d\tau \right]^{1/2} . \quad (15)$$

Fig. 4 shows the behavior of $E_2'(\alpha_{i,0}^{(k)})$ as a function of $\alpha_{i,0}^{(k)}$ for various values of N_i. From the comparison of Figs. 2 and 4, the above-mentioned compensation effect is obvious since the error function $E_2'(\alpha_{i,0}^{(k)})$ is overall much smaller than $E_2(\alpha_{i,0}^{(k)})$. Needless to say, $E_2'(\alpha_{i,0}^{(k)})$ is even symmetrical, i.e., $E_2'(\alpha_{i,0}^{(k)}) = E_2'(-\alpha_{i,0}^{(k)})$, and periodic with period $\alpha_{\mathrm{per}} = \pi/(4N_i)$, i.e., $E_2'(\alpha_{i,0}^{(k)}) = E_2'(\alpha_{i,0}^{(k)} + p\alpha_{\mathrm{per}})$, where $p = \pm 1, \pm 2, \ldots$ The maximum and minimum values of $E_2'(\alpha_{i,0}^{(k)})$ are taken at $\alpha_{i,0}^{(k)} = p\alpha_{\mathrm{per}}$ and $\alpha_{i,0}^{(k)} = (2p+1)\alpha_{\mathrm{per}}/2$, respectively. Note that $E_2'(\alpha_{i,0}^{(k)})$ and $E_2(\alpha_{i,0}^{(k)})$ have different periods and that the maximum of $E_2'(\alpha_{i,0}^{(k)})$ at $\alpha_{i,0}^{(k)} = 0$ is coincident with the minimum of $E_2(\alpha_{i,0}^{(k)})$ at the same position $\alpha_{i,0}^{(k)} = 0$. Consequently, the original MEDS with $\alpha_{i,0}^{(k)} = 0$ results in the worst fitting with respect to the ACF $r_{\mu \mu}(\tau)$ of the complex process $\mu(t)$. This is completely different from the fitting to the ACF $r_{\mu_i \mu_i}(\tau)$ of the inphase (quadrature) component $\mu_i(t)$, in which case the MEDS provides the best fitting result, as can be seen in Figs. 2 and 3. In Fig. 5, plots of the ACF $\tilde{r}_{\mu \mu}^{(k)}(\tau)$ are shown for four selected values of $\alpha_{i,0}^{(k)}$ computed by using the GMEDS$_1$ with $N_i = 20$ and $K = 4$. Note that $\alpha_{i,0}^{(k)} = \pm \pi/160$ ($k = 3$) and $\alpha_{i,0}^{(k)} = \pm \pi/480$ ($k = 1$) represent the best and worst cases, respectively,
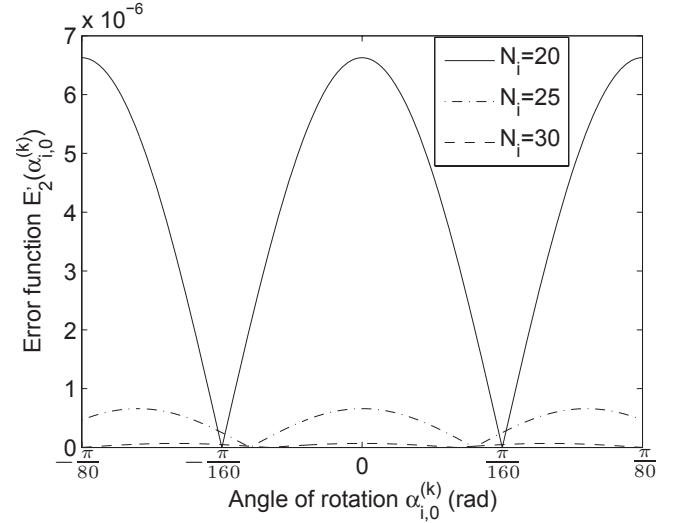
according to (12) and Fig. 4. The even symmetry property is self-evident. The ACF $\tilde{r}_{\mu \mu}^{(k)}(\tau)$ of the simulation model obtained by using the original MEDS ($\alpha_{i,0}^{(k)} = 0$) and the ACF $r_{\mu \mu}(\tau)$ for the reference model are also shown for reasons of comparison. Notice that the performance of the MEDS is worse than the performance of the GMEDS$_1$ in the worst case in terms of the fitting to $r_{\mu \mu}(\tau)$. However, even in the worst case of the GMEDS$_1$, the approximation to $r_{\mu \mu}^{(k)}(\tau)$ is excellent when $\tau \in [0, N_i/(2f_{\max})]$ or, equivalently, $\tau f_{\max} \in [0, 10]$. When $\alpha_{i,0}^{(k)} = \pm \pi/(8N_i) = \pm \pi/160$, the fitting to $r_{\mu \mu}(\tau)$ is excellent even when $\tau_{\max}$ reaches $N_i/f_{\max}$, i.e., $\tau f_{\max} \in [0, 20]$. This is not surprising since this specific constellation corresponds to that of the original MEDS with $2N_i$. In the limited range of $\tau f_{\max} \in [0, 15]$ shown in Fig. 5, the ACF $\tilde{r}_{\mu \mu}^{(k)}(\tau)$ obtained by using the GMEDS$_1$ with $\alpha_{i,0}^{(k)} = \pm \pi/160$ and the ACF $r_{\mu \mu}(\tau)$ of the reference model are indistinguishable.

B. The GMEDS$_2$

In the following, we present another solution to the problem described in Section II by using the GMEDS$_2$. As in the previous subsection, the reference model is again an ideal Rayleigh channel model under isotropic scattering conditions. By using the GMEDS$_2$, we can design a set of K mutually uncorrelated Rayleigh fading waveforms $\tilde{\zeta}^{(k)}(t)$ if the angle of rotation $\alpha_{i,0}^{(k)}$ is given by

$$\alpha_{i,0}^{(k)} = \frac{\alpha_{\mathrm{per}}}{2} \cdot \frac{k-1}{K-1} = \frac{\pi}{4N_i} \cdot \frac{k-1}{K-1} \quad (16)$$

for $k = 1, 2, \ldots, K$ and $i = 1, 2$, where $\alpha_{\mathrm{per}} = \pi/(2N_i)$ and $N_2 := N_1 + 1$. In the following, we analyze the GMEDS$_2$ and give some reasons for choosing (16).

First, we choose $q = 2$ in (11) and study the influence of $\alpha_{i,0}^{(k)}$ on the quality of the approximation in (5). To measure the approximation error, we use again the L_2-norm defined in (6), where $\tau_{\max}$ is now given by $\tau_{\max} = N_i/(4f_{\max})$. The error function $E_2(\alpha_{i,0}^{(k)})$ by using the GMEDS$_2$ is plotted
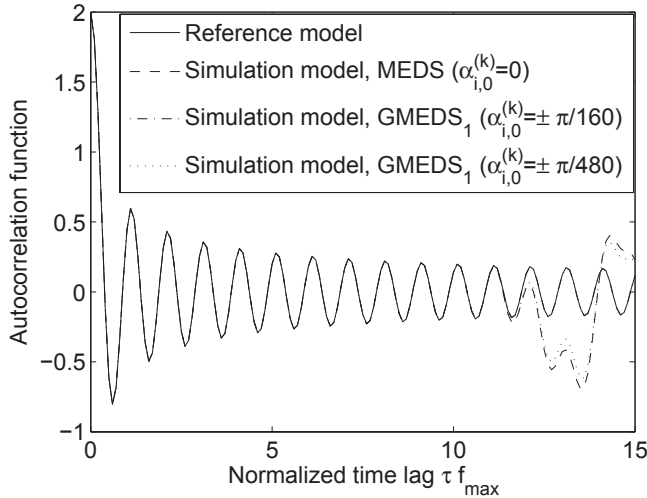
Fig. 5. The ACF $r_{\mu\mu}(\tau)$ of the complex waveform of the reference model in comparison with the corresponding ACF $\tilde{r}_{\mu\mu}^{(k)}(\tau)$ of the simulation model designed by using the MEDS with $\alpha_{i,0}^{(k)} = 0$ and the GMEDS$_1$ with $\alpha_{i,0}^{(k)} = \pm\pi/160$ and $\alpha_{i,0}^{(k)} = \pm\pi/480$ ($N_i = 20$, $K = 4$).

Fig. 6. The error function $E_2(\alpha_{i,0}^{(k)})$ as a function of $\alpha_{i,0}^{(k)}$ by using the GMEDS$_2$ for various values of N_i.

in Fig. 6 for various values of N_i. From this figure, we can realize that $E_2(\alpha_{i,0}^{(k)})$ is periodic with period $\alpha_{\mathrm{per}} = \pi/(2N_i)$. It should also be observed that the L_2-norm $E_2(\alpha_{i,0}^{(k)})$ takes its maximum value at $\alpha_{i,0}^{(k)} = p\,\alpha_{\mathrm{per}}$ and its minimum value at $\alpha_{i,0}^{(k)} = (2p+1)\alpha_{\mathrm{per}}/2$, where p is again an integer. The relationship between the period and the maximum/minimum value of $E_2(\alpha_{i,0}^{(k)})$ by employing the GMEDS$_2$ corresponds with the relationship observed for $E_2'(\alpha_{i,0}^{(k)})$ when using the GMEDS$_1$. Moreover, the even symmetry property is kept for the error function when using the GMEDS$_2$, i.e., $E_2(\alpha_{i,0}^{(k)}) = E_2(-\alpha_{i,0}^{(k)})$. If $\alpha_{i,0}^{(k)} = 0$, it follows from (11) that $f_{i,n}^{(k)} = f_{\max}\cos[\frac{\pi}{N_i}(n-\frac{1}{2})]$. Consequently, $f_{i,n}^{(k)} = -f_{i,N_i+1-n}^{(k)}$ holds for $n = 1, 2, \ldots, N_i/2$ if N_i is even and $n = 1, 2, \ldots, (N_i - 1)/2$ if N_i is odd. Based on the symmetry of the cosine functions in (3), half of the N_i terms are actually redundant. But these redundant terms become apparently effective when $0 < \alpha_{i,0}^{(k)} \leq \alpha_{\mathrm{per}}/2$. In fact, if $\alpha_{i,0}^{(k)}$ equals $\alpha_{\mathrm{per}}/2$ then all terms contribute equally to the performance of the GMEDS$_2$. This explains the behavior of the L_2-norm $E_2(\alpha_{i,0}^{(k)})$ shown in Fig. 6. The performance of the GMEDS$_2$ reaches that of the original MEDS if $\alpha_{i,0}^{(k)}$ approaches $\pm\alpha_{\mathrm{per}}/2$. In the worst case, which is given for $\alpha_{i,0}^{(k)} = 0$, it turns out that the GMEDS$_2$ with N_i terms has exactly the same performance as the original MEDS with $N_i/2$ terms. However, the original MEDS is not suitable for designing efficiently a large number K of uncorrelated waveforms, but the GMEDS$_2$ is, as we will see in the following.

Choosing $\alpha_{i,0}^{(k)}$ as in (16) ensures that the conditions in (8a) and (8b) are fulfilled, so that (7a) and (7b) follow, respectively. An interesting property of the GMEDS$_2$ is that the approximation in (5) is excellent at least over the interval $[0, N_i/(4f_{\max})]$ for all values of $\alpha_{i,0}^{(k)}$. Hence, the proposed GMEDS$_2$ provides a simple closed-form solution to the parameter computation problem by fulfilling the conditions (i) and (ii) for any number K while keeping the complexity low.
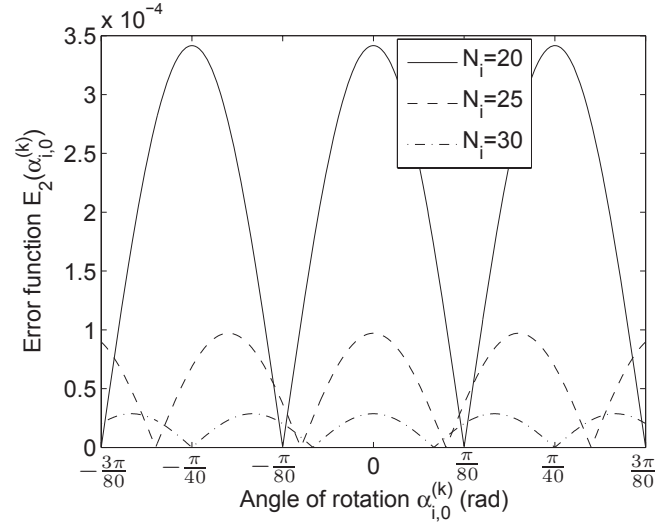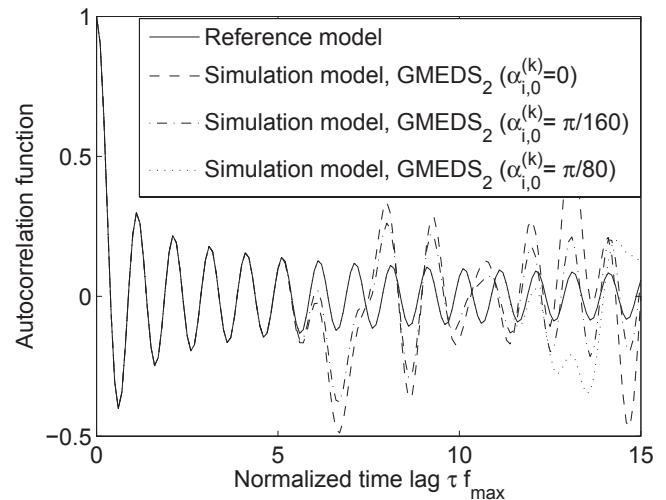

Fig. 7. The ACF $r_{\mu_i\mu_i}(\tau)$ of the quadrature components of the reference model in comparison with the corresponding ACF $\tilde{r}_{\mu_i\mu_i}^{(k)}(\tau)$ of the simulation model by using the GMEDS$_2$ with $N_i = 20$ for various values of the angle of rotation $\alpha_{i,0}^{(k)}$.

Fig. 7 shows plots of the ACF $r_{\mu_i\mu_i}(\tau)$ of the reference model in comparison with the ACF $\tilde{r}_{\mu_i\mu_i}^{(k)}(\tau)$ of the simulation model for various values of $\alpha_{i,0}^{(k)}$ computed according to (16) by choosing $N_i = 20$. Note that the best fitting is obtained if $\alpha_{i,0}^{(k)} = \pi/(4N_i) = \pi/80$, while the worst case occurs if $\alpha_{i,0}^{(k)} = 0$. This is consistent with the conclusions drawn from the results shown in Fig. 6. In Fig. 8, we show the ACF $r_{\mu\mu}(\tau)$ of the reference model and the ACF $\tilde{r}_{\mu\mu}^{(k)}(\tau)$ of the simulation model designed by using the GMEDS$_2$ with the same values of $\alpha_{i,0}^{(k)}$ as in Fig. 7. Finally, Fig. 9 illustrates exemplarily for $K = 3$ the temporal behavior of the resulting three uncorrelated fading envelopes $\tilde{\zeta}^{(k)}(t)$ ($k = 1, 2, 3$).

IV. RELATED PARAMETER COMPUTATION METHODS DERIVED FROM THE GMEDS$_q$

The GMEDS$_q$ actually represents a class of parameter computation methods, which includes the following five well-
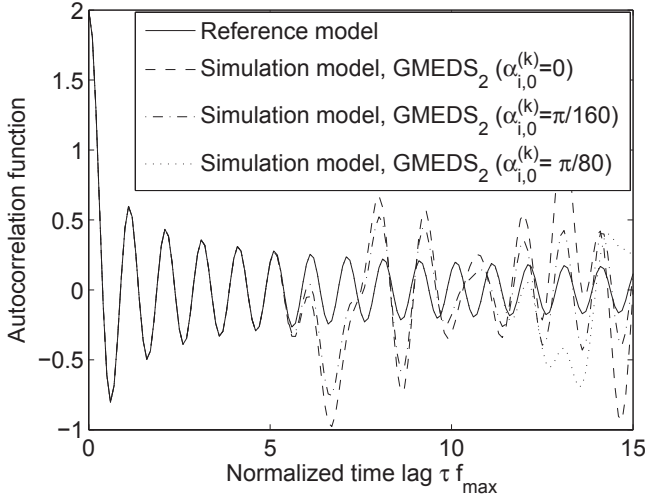
Fig. 8. The ACF $r_{\mu\mu}(\tau)$ of the complex waveform of the reference model in comparison with the corresponding ACF $\tilde{r}_{\mu\mu}^{(k)}(\tau)$ of the simulation model by using the GMEDS$_2$ with $N_1 = 20$ and $N_2 = 21$ for various values of the angle of rotation $\alpha_{i,0}^{(k)}$.
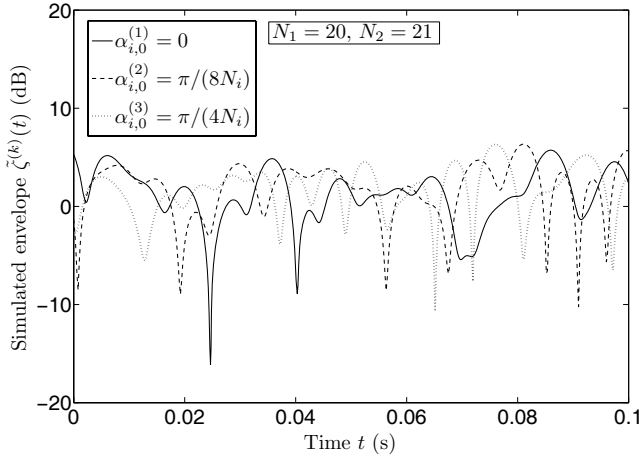

Fig. 9. Simulated uncorrelated Rayleigh fading waveforms $\tilde{\zeta}^{(k)}(t)$ ($k = 1, 2, 3$) by using the GMEDS$_2$ ($f_{\max} = 91\,\text{Hz}$, $N_1 = 20$, $N_2 = 21$).

known methods as special cases.

1) MEDS: The original MEDS [19] results from (11) if $q = 1$ and $\alpha_{i,0}^{(k)} = 0$, but N_i in (11) has to be replaced by $N_i^{(k)}$ in order to generate multiple uncorrelated processes [9], [10]. The discrete frequencies are therefore given by $f_{i,n}^{(k)} = f_{\max} \cos[\pi(n - 1/2)/(2N_i^{(k)})]$. It was shown in [9], [10] that the only way to fulfill (8a) and (8b) with the MEDS is to guarantee that $N_i^{(k)}/N_\lambda^{(l)} \neq (2n - 1)/(2m - 1)$ for all $n = 1, 2, \ldots, N_i^{(k)}$ and $m = 1, 2, \ldots, N_\lambda^{(l)}$. With the increase of the number of simulated uncorrelated fading waveforms, the numbers of sinusoids of the deterministic SOS channel simulator increases exponentially if the MEDS is used. For example, to simulate $K = 4$ uncorrelated Rayleigh fading channels by using the MEDS, a possible set of 8 values for the number of sinusoids N_i fulfilling (8a) and (8b) is $\{8, 9, 10, 12, 16, 32, 64, 128\}$ [10]. This obvious drawback limits the usefulness of the MEDS if a large number of uncorrelated processes is required.

2) MEDS with Set Partitioning (MEDS-SP): Another special case is obtained when $q = 1$ and $\alpha_{i,0}^{(k)} = \pi[k - (K + 1)/2]/(2KN_i)$, which results in the so-called MEDS-SP [18]. This method actually belongs to the GMEDS$_1$, but with a different expression for $\alpha_{i,0}^{(k)}$. The purpose of the MEDS-SP is to take advantage of averaging over multiple sample functions (trials) — a technique that is unavoidable when non-ergodic stochastic methods [12]–[15] are used. In [18], it was shown that the MEDS-SP outperforms the non-ergodic method proposed in [14] with respect to both single trials and multiple trials. The use of the MEDS-SP, without further modifications, is not recommended for the design of multiple uncorrelated Rayleigh fading waveforms.

3) Method of Equal Areas (MEA): The MEA [21] ensues if $q = 1$ and $\alpha_{i,0}^{(k)} = \pi/(4N_i^{(k)})$. It follows that $f_{i,n}^{(k)} = f_{\max} \cos[n\pi/(2N_i^{(k)})]$. Note that the MEA was originally proposed for the design of a single Rayleigh fading waveform. To generate multiple uncorrelated Rayleigh fading waveforms by using the MEA, N_i in (11) has to be replaced by $N_i^{(k)}$. Similar to the MEDS, the only way to fulfill (8a) and (8b) with the MEA is to change the number of sinusoids for different waveforms, which will greatly increase the simulator complexity if a large number of uncorrelated waveforms is required.

4) Randomized MEDS (R-MEDS): Furthermore, the R-MEDS [14] is obtained if $q = 1$ and $\alpha_{i,0}^{(k)}$ is replaced by $\boldsymbol{\alpha}_{i,0}^{(k)} = \boldsymbol{\theta}_i^{(k)}/(4N_i)$, where $\boldsymbol{\theta}_i^{(k)}$ are i.i.d. random variables, each having a uniform distribution over $[-\pi, \pi)$. The R-MEDS and the following MCM can be used to generate a large number of uncorrelated Rayleigh fading waveforms without increasing the simulator's complexity. However, due to the non-ergodicity property of the methods, the resulting simulators are not efficient, as already discussed in [10].

5) Monte Carlo Method (MCM): Finally, if $q = 0$ and $\alpha_{i,0}^{(k)}$ is replaced by $\varphi_{i,n}^{(k)}$ with $\varphi_{i,n}^{(k)}$ being i.i.d. random variables uniformly distributed over $(0, \pi/2]$, then we obtain the MCM, which was originally proposed in [22] and further developed in [13].

V. COMPARISON AND DISCUSSION OF THE GMEDS$_1$ AND THE GMEDS$_2$

Compared with the MEDS, one obvious advantage of both the GMEDS$_1$ and the GMEDS$_2$ is that they can be used to design a very large (theoretically an infinite) number of mutually uncorrelated Rayleigh fading waveforms by keeping the number of sinusoids constant. In fact, the complexity of the resulting channel simulators designed using the proposed two methods is low and independent of the number of generated uncorrelated fading waveforms. The drawback of the GMEDS$_1$ is that small non-negative (non-positive) errors have to be accepted concerning the fitting of the ACF of the inphase (quadrature) component of the generated complex waveforms. However, these errors compensate each other over the domain of interest when considering the ACF of the resulting complex waveform. Note that the performance

of many communication systems, such as differential phase shift keying (DPSK) modulation [3] and orthogonal frequency division multiplexing (OFDM) systems [4], depends only on the ACF of the complex waveform, rather than the ACFs of the quadrature components. Therefore, the GMEDS$_1$ is applicable to such systems.

At the price of increased complexity, the GMEDS$_2$ enables an excellent fitting to both the quadrature ACFs and the ACF of the complex waveform over the domain of interest. Note that for the GMEDS$_2$, the domain of interest is only one half of that for the GMEDS$_1$. However, this does not diminish the usefulness of the resulting channel simulator because the performance of most mobile communication systems is only sensitive to errors of the ACF if the time lag is small, meaning $\tau f_{\max} \leq 0.3$ [23]. For such systems, the GMEDS$_2$ should be preferred to the GMEDS$_1$.

The results of a detailed comparative performance study of the GMEDS$_1$ and the GMEDS$_2$ are shown in Tables I and II. Table I presents the values of the error function $E_2(\alpha_{i,0}^{(k)})$ obtained by using the GMEDS$_1$ with $N_1 = N_2 = 20$ and the GMEDS$_2$ with $N_1 = 20$ and $N_2 = 21$. In Table II, the corresponding results of the error function $E_2'(\alpha_{i,0}^{(k)})$ are shown. In all cases, we have chosen $K = 3$ and $f_{\max} = 91$ Hz. From the results shown in Table I, we can clearly conclude that the GMEDS$_2$ outperforms the GMEDS$_1$ with respect to the fitting of the ACF of the inphase (quadrature) component if $\tau_{\max}$ is set to $N_i/(4f_{\max})$. If $\tau_{\max} = N_i/(2f_{\max})$, then it turns out that the GMEDS$_1$ performs better than the GMEDS$_2$ except for the case when $k = K$. Table II shows that the GMEDS$_1$ in general outperforms the GMEDS$_2$ with respect to the error function $E_2'(\alpha_{i,0}^{(k)})$, which measures the accuracy of the channel simulator's ACF of the complex generated waveform.

In addition, we have compared the performance of the GMEDS$_1$ and GMEDS$_2$ with the modified MEDS (MMEDS), which has recently been proposed in [11]. According to the results shown in Tables I and II, we can conclude that the MMEDS is in general better than the GMEDS$_1$ and GMEDS$_2$ in terms of the fitting of the ACF of the inphase (quadrature) component for both $\tau_{\max} = N_i/(2f_{\max})$ and $\tau_{\max} = N_i/(4f_{\max})$. For the fitting of the ACF of the complex waveform, both the GMEDS$_1$ and MMEDS are in general superior to the GMEDS$_2$, while the GMEDS$_1$ has a slightly better performance than the MMEDS.

Next, we study the performance of the proposed methods under limited simulation time constraints. That is, we assume that the simulation of $\tilde{\mu}_i^{(k)}(t)$ starts at $t_1 = -T$ and ends at $t_2 = +T$, where T is limited ($T < \infty$). Under this condition, the processes $\tilde{\mu}_i^{(k)}(t)$ and $\tilde{\mu}_\lambda^{(l)}(t)$ are correlated even when the unequalities in (8a) and (8b) are fulfilled. To study the effect of limited simulation time, we define the following correlation coefficient

$$\tilde{c}_{\mu_i\mu_\lambda}^{(k,l)} := \frac{1}{2T} \int_{-T}^{T} \tilde{\mu}_i^{(k)}(t)\, \tilde{\mu}_\lambda^{(l)}(t)\, dt, \quad 0 < T < \infty. \quad (17)$$

Notice that the correlation coefficient $\tilde{c}_{\mu_i\mu_\lambda}^{(k,l)}$ equals the CCF $\tilde{r}_{\mu_i\mu_\lambda}^{(k,l)}(\tau)$ at $\tau = 0$ under the condition that T is limited

[cf. (4)]. Substituting (2) in (17) gives the closed-form solution

$$\tilde{c}_{\mu_i\mu_\lambda}^{(k,l)} = \frac{1}{2\pi T \sqrt{N_i N_\lambda}} \sum_{n=1}^{N_i} \sum_{m=1}^{N_\lambda}$$
$$\left[\frac{\sin(2\pi(f_{i,n}^{(k)} - f_{\lambda,m}^{(l)})T)\cos(\theta_{i,n}^{(k)} - \theta_{\lambda,m}^{(l)})}{f_{i,n}^{(k)} - f_{\lambda,m}^{(l)}} \right.$$
$$\left. + \frac{\sin(2\pi(f_{i,n}^{(k)} + f_{\lambda,m}^{(l)})T)\cos(\theta_{i,n}^{(k)} + \theta_{\lambda,m}^{(l)})}{f_{i,n}^{(k)} + f_{\lambda,m}^{(l)}} \right]. \quad (18)$$

Obviously, the quantity $\tilde{c}_{\mu_i\mu_\lambda}^{(k,l)}$ depends on all model parameters, including the phases $\theta_{i,n}^{(k)}$ and T. For our purpose, it is sufficient to focus on the upper limit of $\tilde{c}_{\mu_i\mu_\lambda}^{(k,l)}$. Let us denote the upper limit by $\hat{c}_{\mu_i\mu_\lambda}^{(k,l)}$, then it follows from (18) by using $\sin(x) \leq 1$ and $\cos(x) \leq 1$ that

$$\hat{c}_{\mu_i\mu_\lambda}^{(k,l)} = \frac{1}{\pi T \sqrt{N_i N_\lambda}} \sum_{n=1}^{N_i} \sum_{m=1}^{N_\lambda} \frac{f_{i,n}^{(k)}}{(f_{i,n}^{(k)})^2 - (f_{\lambda,m}^{(l)})^2}. \quad (19)$$

It is apparent that $\hat{c}_{\mu_i\mu_\lambda}^{(k,l)} \to 0$ as $T \to \infty$. In practise, however, the simulation time $T_{\mathrm{sim}} = 2T$ is limited, and thus the theoretical uncorrelated processes $\tilde{\mu}_i^{(k)}(t)$ and $\tilde{\mu}_\lambda^{(l)}(t)$ remain correlated. The evaluation results of the upper limit $\hat{c}_{\mu_i\mu_\lambda}^{(k,l)}$ are listed in Table III for the GMEDS$_1$, GMEDS$_2$, and MMEDS. The results clearly show that under practical aspects the GMEDS$_1$ and GMEDS$_2$ are superior to the MMEDS, as the latter method results in deterministic processes $\tilde{\mu}_i^{(k)}(t)$ and $\tilde{\mu}_\lambda^{(l)}(t)$ which decorrelate very slowly with increasing values of T. The reason is that the MMEDS [11] clusters the discrete Doppler frequencies $f_{i,n}^{(k)}$ tightly around the optimum (original MEDS [19]) for $k = 1, 2, \ldots, K$. This keeps the frequency differences in the denominator of (19) very small and results thus in large values for $\hat{c}_{\mu_i\mu_\lambda}^{(k,l)}$. This drawback is avoided by the GMEDS$_1$ and GMEDS$_2$, where the spread of the discrete Doppler frequencies $f_{i,n}^{(k)}$ is much larger.

Finally, we mention that for both the GMEDS$_1$ and GMEDS$_2$, the domain of interest increases linearly with the number of sinusoids and can thus easily be controlled. It should be highlighted that both methods result in closed-form expressions [see (11) in combination with (12) and (16)] for the model parameters, which have been derived in our paper by assuming isotropic scattering conditions. The extension of the proposed techniques to wireless non-isotropic channels might be a topic for future research.

For some applications, it is desirable to generate multiple fading envelopes with specified cross-correlation functions. This is important, e.g., for studying the effects caused by correlated sub-channels on the capacity of MIMO systems. One straightforward method is to employ a linear combination of multiple uncorrelated processes [4], [24]. In line with the idea in [24], the deterministic SOS channel simulator with the newly developed methods can be extended to generate multiple cross-correlated Rayleigh fading waveforms for the simulation of more realistic MIMO channels. Finally, it should be mentioned that a detailed comparison of the MEDS with the L_p-norm method and various random methods in [14]–[16] can be found in [10].

TABLE I
ERROR FUNCTION $E_2(\alpha_{i,0}^{(k)})$ OBTAINED BY USING THE GMEDS$_1$ ($N_1 = N_2 = 20$), THE GMEDS$_2$ ($N_1 = 20$, $N_2 = 21$), AND THE MMEDS [11] ($N_1 = N_2 = 20$) WITH $K = 3$ AND $f_{max} = 91$ Hz.

Method	τ_{max}	$E_2(\alpha_{1,0}^{(1)})/E_2(\alpha_{2,0}^{(1)})$	$E_2(\alpha_{1,0}^{(2)})/E_2(\alpha_{2,0}^{(2)})$	$E_2(\alpha_{1,0}^{(3)})/E_2(\alpha_{2,0}^{(3)})$
GMEDS$_1$	$N_i/(2f_{max})$	0.0094/0.0094	0.0176/0.0176	0.0239/0.0239
GMEDS$_2$	$N_i/(2f_{max})$	0.1438/0.1413	0.1017/0.0999	$2.6877 \cdot 10^{-6}/1.6880 \cdot 10^{-6}$
GMEDS$_1$	$N_i/(4f_{max})$	0.0065/0.0065	0.0129/0.0129	0.0191/0.0191
GMEDS$_2$	$N_i/(4f_{max})$	$3.4164 \cdot 10^{-4}/2.6462 \cdot 10^{-4}$	$2.4157 \cdot 10^{-4}/1.8711 \cdot 10^{-4}$	$2.5420 \cdot 10^{-16}/3.0724 \cdot 10^{-16}$
MMEDS [11]	$N/(2f_{max})$	$2.6218 \cdot 10^{-6}/2.6336 \cdot 10^{-6}$	$2.6218 \cdot 10^{-6}/2.6336 \cdot 10^{-6}$	$2.6218 \cdot 10^{-6}/2.6336 \cdot 10^{-6}$
MMEDS [11]	$N/(4f_{max})$	$4.1128 \cdot 10^{-8}/4.1128 \cdot 10^{-8}$	$4.1128 \cdot 10^{-8}/4.1128 \cdot 10^{-8}$	$4.1128 \cdot 10^{-8}/4.1128 \cdot 10^{-8}$

TABLE II
ERROR FUNCTION $E_2'(\alpha_{i,0}^{(k)})$ OBTAINED BY USING THE GMEDS$_1$ ($N_1 = N_2 = 20$), THE GMEDS$_2$ ($N_1 = 20$, $N_2 = 21$), AND THE MMEDS [11] ($N_1 = N_2 = 20$) WITH $K = 3$ AND $f_{max} = 91$ Hz.

Method	τ_{max}	$E_2'(\alpha_{i,0}^{(1)})$	$E_2'(\alpha_{i,0}^{(2)})$	$E_2'(\alpha_{i,0}^{(3)})$
GMEDS$_1$	$N_1/(2f_{max})$	$4.3488 \cdot 10^{-6}$	$1.6611 \cdot 10^{-6}$	$1.6611 \cdot 10^{-6}$
GMEDS$_2$	$N_1/(2f_{max})$	0.1398	0.0988	$2.8018 \cdot 10^{-6}$
GMEDS$_1$	$N_1/(4f_{max})$	$3.8978 \cdot 10^{-16}$	$3.5944 \cdot 10^{-16}$	$3.8696 \cdot 10^{-16}$
GMEDS$_2$	$N_1/(4f_{max})$	$2.7468 \cdot 10^{-4}$	$1.9423 \cdot 10^{-4}$	$3.8083 \cdot 10^{-16}$
MMEDS [11]	$N/(2f_{max})$	$5.2541 \cdot 10^{-6}$	$5.2541 \cdot 10^{-6}$	$5.2541 \cdot 10^{-6}$
MMEDS [11]	$N/(4f_{max})$	$1.4885 \cdot 10^{-14}$	$1.4885 \cdot 10^{-14}$	$1.4885 \cdot 10^{-14}$

TABLE III
UPPER LIMIT $\hat{c}_{\mu_i\mu_\lambda}^{(k,l)}$ OF THE CORRELATION COEFFICIENT OF $\tilde{\mu}_i^{(k)}(t)$ AND $\tilde{\mu}_\lambda^{(l)}(t)$ UNDER LIMITED SIMULATION TIME CONSTRAINTS BY USING THE GMEDS$_1$ ($N_1 = N_2 = 20$), THE GMEDS$_2$ ($N_1 = 20$, $N_2 = 21$), AND THE MMEDS [11] ($N_1 = N_2 = 20$) WITH $K = 3$ AND $f_{max} = 91$ Hz.

$\hat{c}_{\mu_i\mu_\lambda}^{(k,l)}$	GMEDS$_1$	GMEDS$_2$	MMEDS [11]
$\hat{c}_{\mu_1\mu_1}^{(1,2)}$	0.6765s/T	$-5.0889 \cdot 10^{-16}$s/T	$-1.5915 \cdot 10^{6}$s/T
$\hat{c}_{\mu_1\mu_1}^{(1,3)}$	0.3249s/T	$-1.4843 \cdot 10^{-16}$s/T	$-7.9577 \cdot 10^{5}$s/T
$\hat{c}_{\mu_1\mu_1}^{(2,3)}$	0.6391s/T	0.2070s/T	$-1.5915 \cdot 10^{6}$s/T
$\hat{c}_{\mu_2\mu_2}^{(1,2)}$	-0.8293s/T	$-5.0889 \cdot 10^{-16}$s/T	$1.5915 \cdot 10^{6}$s/T
$\hat{c}_{\mu_2\mu_2}^{(1,3)}$	-0.4103s/T	$-1.4843 \cdot 10^{-16}$s/T	$7.9577 \cdot 10^{5}$s/T
$\hat{c}_{\mu_2\mu_2}^{(2,3)}$	-1.0062s/T	0.2070s/T	$1.5915 \cdot 10^{6}$s/T
$\hat{c}_{\mu_1\mu_2}^{(1,1)}$	-0.3035s/T	$-1.6554 \cdot 10^{-16}$s/T	$7.9577 \cdot 10^{5}$s/T
$\hat{c}_{\mu_1\mu_2}^{(2,2)}$	-0.0817s/T	0.2882s/T	$3.9789 \cdot 10^{5}$s/T
$\hat{c}_{\mu_1\mu_2}^{(3,3)}$	0.0386s/T	1.0993s/T	$2.6526 \cdot 10^{5}$s/T

methods are useful for the design of simulation models for diversity-combined Rayleigh fading channels, amplify-and-forward fading channels, frequency-selective channels, and MIMO channels with uncorrelated sub-channels.

VI. CONCLUSION

In this paper, we have introduced the so-called GMEDS$_q$ as a new class of parameter computation methods for the design of deterministic SOS-based Rayleigh fading channel simulators. This class of methods includes several other well-known parameter computation methods as special cases, e.g., the original MEDS, the MEDS-SP, the R-MEDS, the MEA, and the MCM. Two new special cases, namely the GMEDS$_1$ and the GMEDS$_2$, have been proposed to generate a large number of multiple uncorrelated Rayleigh fading waveforms without increasing the model complexity. A detailed comparison of the GMEDS$_1$ and the GMEDS$_2$ demonstrates that the former one has a slightly better overall performance over a wider range of time lag values. The GMEDS$_1$ is especially suitable for the design of channel simulators for communication systems whose performance depends only on the ACF of the complex waveform, rather than the ACFs of the quadrature components. If this is not the case for the communication system under study, then we recommend using the GMEDS$_2$. Both

REFERENCES

[1] S. O. Rice, "Mathematical analysis of random noise," *Bell Syst. Tech. J.*, vol. 23, pp. 282-332, July 1944.

[2] S. O. Rice, "Mathematical analysis of random noise," *Bell Syst. Tech. J.*, vol. 24, pp. 46-156, Jan. 1945.

[3] W. C. Jakes, ed., *Microwave Mobile Communications*. New Jersey: IEEE Press, 1994.

[4] G. L. Stüber, *Principles of Mobile Communications*. Boston: Kluwer Academic Publishers, 2nd ed., 2001.

[5] P. Dent, G. E. Bottomley, and T. Croft, "Jakes fading model revisited," *Electron. Lett.*, vol. 29, no. 13, pp. 1162-1163, June 1993.

[6] Y. B. Li and Y. L. Guan, "Modified Jakes model for simulating multiple uncorrelated fading waveforms," in *Proc. IEEE ICC'00*, New Orleans, LA, USA, June 2000, pp. 46-49.

[7] Y. X. Li and X. J. Huang, "The simulation of independent Rayleigh faders," *IEEE Trans. Commun.*, vol. 50, no. 9, pp. 1503-1514, Sept. 2002.

[8] M. Pätzold, *Mobile Fading Channels*. Chichester: John Wiley & Sons, 2002.

[9] C.-X. Wang and M. Pätzold, "Methods of generating multiple uncorrelated Rayleigh fading processes," in *Proc. IEEE VTC 2003-Spring*, Jeju, Korea, Apr. 2003, pp. 510-514.

[10] C.-X. Wang, M. Pätzold, and D. Yuan, "Accurate and efficient simulation of multiple uncorrelated Rayleigh fading waveforms," *IEEE Trans. Wireless Commun.*, vol. 6, no. 3, pp. 833-839, Mar. 2007.

[11] C.-X. Wang, D. Yuan, H. H. Chen, and W. Xu, "An improved deterministic SoS channel simulator for multiple uncorrelated Rayleigh fading channels," *IEEE Trans. Wireless Commun.*, vol. 7, no. 9, pp. 3307-3311, Sept. 2008.

[12] A. G. Zajić and G. L. Stüber, "Efficient simulation of Rayleigh fading with enhanced de-correlation properties," *IEEE Trans. Wireless Commun.*, vol. 5, no. 7, pp. 1866–1875, July 2006.

[13] P. Höher, "A statistical discrete-time model for the WSSUS multipath channel," *IEEE Trans. Veh. Technol.*, vol. 41, no. 4, pp. 461-468, Nov. 1992.

[14] Y. R. Zheng and C. S. Xiao, "Improved models for the generation of multiple uncorrelated Rayleigh fading waveforms," *IEEE Commun. Lett.*, vol. 6, no. 6, pp. 256-258, June 2002.

[15] Y. R. Zheng and C. S. Xiao, "Simulation models with correct statistical properties for Rayleigh fading channels," *IEEE Trans. Commun.*, vol. 51, no. 6, pp. 920-928, June 2003.

[16] C. S. Patel, G. L. Stüber, and T. G. Pratt, "Comparative analysis of statistical models for the simulation of Rayleigh faded cellular channels," *IEEE Trans. Commun.*, vol. 53, no. 6, pp. 1017-1026, June 2005.

[17] M. Pätzold, "On the stationarity and ergodicity of fading channel simulators based on Rice's sum-of-sinusoids," *International J. Wireless Inform. Networks*, vol. 11, no. 2, pp. 63-69, Apr. 2004.

[18] M. Pätzold, B. O. Hogstad, and D. Kim, "A new design concept for high-performance fading channel simulators using set partitioning," *Wireless Personal Commun.*, vol. 40, no. 2, pp. 267-279, Feb. 2007.

[19] M. Pätzold, U. Killat, F. Laue, and Y. Li, "On the statistical properties of deterministic simulation models for mobile fading channels," *IEEE Trans. Veh. Technol.*, vol. 47, no. 1, pp. 254-269, Feb. 1998.

[20] R. H. Clarke, "A statistical theory of mobile-radio reception," *Bell Syst. Tech. J.*, vol. 47, pp. 957-1000, July/Aug. 1968.

[21] M. Pätzold, U. Killat, and F. Laue, "A deterministic digital simulation model for Suzuki processes with application to a shadowed Rayleigh land mobile radio channel," *IEEE Trans. Veh. Technol.*, vol. 45, no. 2, pp. 318-331, May 1996.

[22] H. Schulze, "Stochastische Modelle und digitale Simulation von Mobilfunkkanälen," in *Proc. Kleinheubacher Reports German PTT* , Darmstadt, Germany, 2003, vol. 32, pp. 473-483.

[23] P. Hoeher and A. Steingass, "Modeling and emulation of multipath fading channels using controlled randomness," in *Proc. ITG-Fachtagung "Wellenausbreitung bei Funksystemen und Mikrowellensystemen"*, Oberpfaffenhofen, Germany, May 1998, pp. 209-220.

[24] C.-X. Wang and M. Pätzold, "Efficient simulation of multiple cross-correlated Rayleigh fading channels," in *Proc. IEEE PIMRC'03*, Beijing, China, Sept. 2003, pp. 1526-1530.

Matthias Pätzold received the Dipl.-Ing. and Dr.-Ing. degrees in electrical engineering from Ruhr-University Bochum, Bochum, Germany, in 1985 and 1989, respectively, and the habil. degree in communications engineering from the Technical University of Hamburg-Harburg, Germany, in 1998. From 1990 to 1992, he was with ANT Nachrichtentechnik GmbH, Backnang, Germany, where he was engaged in digital satellite communications. From 1992 to 2001, he was with the department of digital networks at the Technical University Hamburg-Harburg. Since 2001, he has been a full professor of mobile communications with the University of Agder, Norway. He authored several books and numerous technical papers. His publications received eight best paper awards. He has been actively participating in numerous conferences serving as TPC chair and TPC member for more than 10 conferences within the recent three years.

Cheng-Xiang Wang (S'01-M'05-SM'08) received the BSc and MEng degrees in communication and information systems from Shandong University, China, in 1997 and 2000, respectively, and the PhD degree in wireless communications from Aalborg University, Denmark, in 2004.

Dr Wang has been a lecturer at Heriot-Watt University, Edinburgh, UK since 2005. He is also an honorary fellow of the University of Edinburgh, UK, a guest researcher of Xidian University, China, and an adjunct professor of Guilin University of Electronic Technology, China. He was a research fellow at the University of Agder, Norway, from 2001-2005, a visiting researcher at Siemens AG-Mobile Phones, Munich, Germany, in 2004, and a research assistant at Technical University of Hamburg-Harburg, Germany, from 2000-2001. His current research interests include wireless channel modelling and simulation, cognitive radio networks, mobile-to-mobile communications, cooperative communications, cross-layer design, MIMO, OFDM, UWB, wireless sensor networks, and (beyond) 4G. He has published 1 book chapter and over 100 papers in journals and conferences.

Dr Wang serves as an editor for IEEE TRANSACTIONS ON WIRELESS COMMUNICATIONS, WILEY WIRELESS COMMUNICATIONS AND MOBILE COMPUTING JOURNAL, WILEY SECURITY AND COMMUNICATION NETWORKS JOURNAL, and JOURNAL OF COMPUTER SYSTEMS, NETWORKS, AND COMMUNICATIONS. He served or is servings as a TPC chair for CMC 2009, publicity chair for CrownCom 2009, TPC symposium co-chair for IWCMC 2009, General Chair for VehiCom 2009, and TPC vice-chair or member for more than 35 international conferences. Dr Wang is listed in *Dictionary of International Biography 2008*, *Who's Who in the World 2008 and 2009*, and *Great Minds of the 21st Century 2009*.

Bjørn Olav Hogstad received the cand.scient degree in applied and industrial mathematics from the University of Oslo, Norway, in 1999, and the PhD degree in wireless communications from Aalborg University, Denmark, in 2008. He also completed a one year study of pedagogic at Agder University College, Kristiansand, Norway, in 2001. After graduating from the University of Oslo in 1999, he worked for almost two years as a college teacher. From 2002 to 2003 he worked as an assistant professor of mathematics and informatics at the Faculty of Engineering and Science of Agder University College. From 2003 to 2007, he was a research fellow of mobile communications with Agder University College, Grimstad, Norway. Since 2008, he has been a member of the Department of Electronics and Communications at Centro de Estudios e Investigaciones Técnicas de Gipuzkoa (CEIT), San Sebastián, Spain. He is also an associate professor at Engineering School of the University of Navarra (Tecnun). His current research interests include mobile fading channel modelling and capacity analysis of multiple-input multiple-output (MIMO) systems. Together with Matthias Pätzold, Bjørn Olav Hogstad received the "Best Paper Award" of the 8th International Symposium on Wireless Personal Multimedia Communications (WPMC'05) in Aalborg, Denmark and the "Best Paper Award" of the 3rd International Symposium on Wireless Communication Systems (ISWCS'06) in Valencia, Spain.